Electronic properties and bonding configuration at the TiN/MgO(001) interface

D. Chen, X. L. Ma, Y. M. Wang, and L. Chen
Shenyang National Laboratory for Materials Science, Institute of Metal Research, Chinese Academy of Sciences, Shenyang 110016, China

(Received 18 November 2003; revised manuscript received 2 February 2004; published 1 April 2004)

Growth modes of a TiN thin film, epitaxially grown on MgO(001) substrate, have been proposed on the basis of transmission electron microscopic observation and theoretical calculations. The first-principle plane wave pseudopotential method, based on density functional theory, is applied to calculate electronic properties and bonding configurations at the interface. The theoretical calculations within framework of the observed orientation relationships show that cation-anion bonding across the TiN/MgO(001) interface is favorable. Interfacial structures for this heteroepitaxial system have been established.

DOI: 10.1103/PhysRevB.69.155401 PACS number(s): 73.20.−r, 68.37.Lp, 31.15.Ew, 68.35.Ct

I. INTRODUCTION

Thin films of titanium nitride have attracted much attention because of its superior properties such as high melting point, ultrahardness, and good electrical and thermal conductivity. They are also used extensively as wear-resistant coatings in the cutting and forming tool industry and diffusion barriers in the microelectronics industry.

TiN films have been extensively grown on MgO substrate based on consideration of the same lattice type and small mismatch between their lattice parameters.[1–5] Interfacial structures are of importance because of their potential influence on various properties. Interfacial structures contain two aspects: first, an orientation relationship between film and substrate; and second, atomistic bonding across the interface. The publications on TiN/MgO so far focused mainly on technological and crystallographic issues of this heterosystem; neither experimental nor theoretical work has been done on electronic properties and bonding configurations across the interface. Recently, first-principle calculations based on the density-functional theory have been applied to several metal-ceramic interface systems such as Ag/MgO,[6,7,8] Cu/MgO,[8] Ni/MgO,[8] and Pd/MgO.[9] The first principles pseudopotential method has been proven to be able to provide insight into the bonding nature at an atomistic level that is rather difficult to discern through current microscopic techniques. In the present work, we have combined a first-principle calculation together with high-resolution electron microscopy (HREM) and established fine structures at the interface between TiN thin film and MgO substrate.

II. EXPERIMENTAL AND COMPUTATIONAL DETAILS

A molecular beam epitaxy system, equipped with an electron-cyclotron-resonance bucket ion source, was used for the film growth in the present work. The MgO(001) substrate was cleaned by degreasing and then heated up to 800 °C in the molecular beam epitaxy chamber just before the growth. Titanium was first vaporized by an electron beam evaporator. Nitrogen gas was activated by the ion source and irradiated normal to the MgO substrate surface. Thin foils for cross-section HREM observation were prepared by the conventional method: i.e., by slicing, grinding, dimpling, and finally ion milling. A JEOL 2010 high-resolution electron microscope operated at 200KV was used for microstructural characterization.

The plane wave pseudopotential (PWPP) method was employed to study the structural properties and electronic structure of the bulk TiN, bulk MgO, and the TiN/MgO(001) interface. The program for theoretical calculations in the present work is CASTEP based on density functional theory (DFT) with a PWPP code.[10]

The energy cutoff is 350 eV (25.7 Ry), which means the degree of convergence of any computed property with respect to the quality of the plane wave basis set[11] and the number of special k points employed within the irreducible wedge of the Brillouin zone using the Monkhorst-Pack scheme.[12] The total energy of the system using a planewave basis set is minimized by means of a conjugate gradient technique.[13] The ultrasoft pseudopotentials[14] were taken from the atomic configurations of magnesium, oxygen, titanium, and nitrogen. These pseudopotentials were optimized in order to reduce the size of the planewave basis set. In the calculations, the core radii for the magnesium, oxygen, titanium and nitrogen pseudopotentials were 1.6, 1.5, 1.5, and 1.35 Å, respectively. The Mg $1s$ and $2s$, O $1s$, Ti $1s$, $2s$ and $2p$, and N $1s$ electrons were treated as core electrons, and all the others were treated as valence electrons. The generalized gradient approximation (GGA) was used for all the atomic calculations and the formation of the pseudopotentials. The most frequently used functional form of the GGA is PW91,[15] which has been proven to be well working.[16] The density-mixing scheme based on the Pulay algorithm[17] is used for self-consistent field (SCF) calculation. The SCF tolerance is set at 1×10^{-6} eV/atom.

Before applying PWPP method to the TiN/MgO interface, we first employed such method to calculate lattice constants and modulus for the bulk form of MgO and TiN. It is seen from Table I that the calculated results in the present study agree well with experiments and calculations based on other theories. The well agreements in the bulk forms lend confidence to carry out calculations for the TiN/MgO(001) interface.

TABLE I. Lattice constant and bulk modulus of MgO and TiN according to earlier experiment and recent calculations based on various methods.

	a (Å)	B_0 (GPa)	Method	Ref.
MgO	4.210	160	Expt.	18
	4.205	180	HF[a]	19
	4.171	154	GGA[b]	20
	4.248	153	FP KKR[c]	21
	4.275	145	PP[d]	16
	4.266	149	PP, PW91	This study
TiN	4.240	288	Expt.	22
	4.236	282	PP[d]	16
	4.250	282	T. M. PP[e]	23
	4.319	304	T. M. PP[e]	24
	4.159	310	AEPP[f]	25
	4.233	281	PP, PW91	This study

[a]Periodic Hartree-Fock theory.
[b]Generalized gradient approximation function.
[c]Full potential Korrinag-Kohn-Rostoker Green's function.
[d]Ultrasoft pseuodopotential.
[e]Troullier and Martins pseuodopotential.
[f]All-Electron pseuodopotential.

III. RESULTS AND DISCUSSION

A. Transmission electron microscopy of the TiN/MgO (001) interface

Figure 1 shows a low magnification bright-field image of the TiN/MgO(001) interface obtained with the electron beam along MgO[100] axis. Both MgO and TiN have a NaCl-type structure with lattice parameters of $a_{\mathrm{MgO}}=0.421$ and $a_{\mathrm{TiN}}=0.424$ nm, respectively. The epitaxial growth of TiN film on the MgO substrate is confirmed by selected-area diffraction patterns as well as by high-resolution electron microscopic images. The growth was governed by the orientation relationships of (001)TiN//(001)MgO, (010)TiN//(010)MgO, and (100)TiN//(100)MgO. Cross-sectional HREM images obtained from the [100] direction are shown in Fig. 2. It is clearly seen that the TiN was epitaxially grown on MgO substrate. Misfit dislocations are not observed due to the very small mismatch of their lattice parameters forming a coherent interface.

B. Interface growth modes and their corresponding interfacial energies

Electron diffraction and high-resolution imaging have provided three-dimensional orientation relationships between TiN and MgO. However, HREM imaging, even jointly with image-simulation, cannot clarify atomistic bonding configurations across the interface, which can be proposed as four growth modes as schematically illustrated in Fig. 3 for the TiN/MgO(001) interfaces. The four possible bonding configurations of TiN on MgO(001) are distinguished by the cation-anion counterpart (mode I), the cation-cation counterpart (mode II), the ion-side gap site (the middle of two nearest-neighbor atoms along [010]) (mode III), and the ion-center gap site (the mid of two nearest-neighbor atoms along [110]) (mode IV). Since the slab geometry associated with an undesirable complication about the free surfaces of TiN and MgO,[26] the supercell of multiplayer geometry was chosen with three-dimensional periodicity and two identical interfaces per unit cell. The repeated supercell geometry was denoted by the notation $(n+n)$, where n is the number of atomic layers in the TiN or MgO geometry.

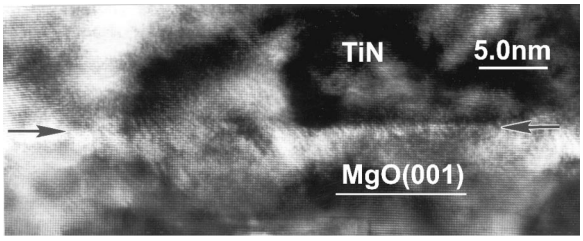

FIG. 1. Low magnification bright-field image of the TiN/MgO(001) interface obtained with the electron beam along the MgO[100] axis.

By performing an iterative process, geometry optimization allows us to refine the geometry of a structure to obtain a stable structure, in which the coordinates of the atoms and possibly the supercell parameters are adjusted so that the total energy of the structure is minimized. In general, the process of geometry optimization typically requires the calculation of different configurations to deduce structural parameters, physical properties, and energetics of the ordering process, and finally results in a model structure that closely resembles the real structure. Its main advantage is that it allows the modelling of the local distortions or displacements. Our geometry optimization calculations for the four possible modes were performed in which all structural parameters not constrained by the space group symmetry were relaxed. After relaxation, the remaining forces on the atoms were less than 0.03 eV/Å, and the remaining stress was less than 0.05 GPa.

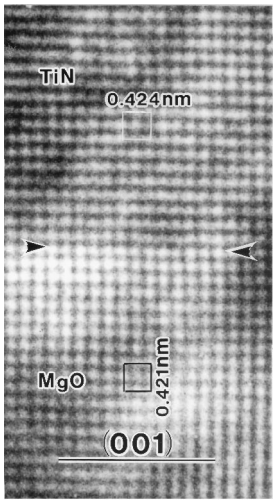

FIG. 2. Cross-sectional HREM images obtained from the [100] direction for the TiN/MgO(001) interface.

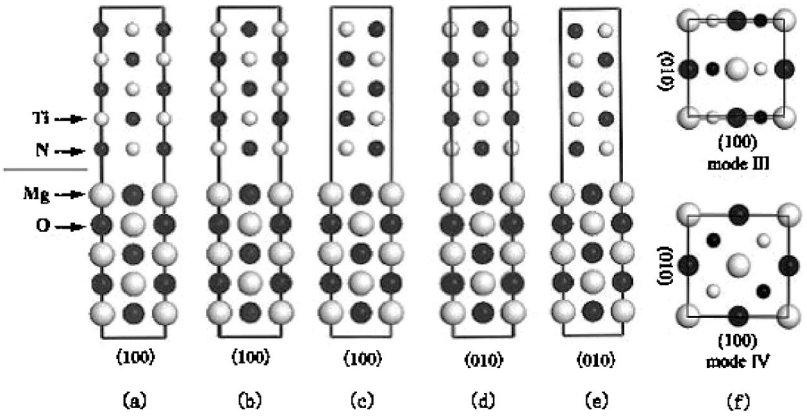

FIG. 3. Side and top views of four growth supercell modes for the TiN/MgO interface proposed according to experimental HREM images. (a) Cation-anion bonding across the interface at (100). (b) Cation-cation and anion-anion bonding at (100). (c) and (d) Ion-side gap site bonding at (100) and (010). (c) and (e) Ion-center gap site bonding at (100) and (010). (f) Top views of Mode III and Mode IV.

The interfacial energy between the two constituents (oxide and nitride) is the dominant energy term and is mainly affected by chemical bonding at a certain lattice match and layer thickness. From each relaxed configuration, we can obtain the minimization of the total energy for different modes, which is responsible for phase stabilization. The smaller the interfacial energy, the more stable the interface structure. The interface energy (E_{inter}) of superlattices can be expressed in the form:

$$E_{\text{inter}}=\frac{1}{2S}\{E_{\text{tot}}[(\text{TiN})_n/(\text{MgO})_n](N1,N2)-N1E_{\text{MgO}}^{\text{bulk}} - N2E_{\text{TiN}}^{\text{bulk}}\}, \quad (1)$$

where energy $E_{\text{tot}}[(\text{TiN})_n/(\text{MgO})_n](N1,N2)$ is the total energy per periodic unit cell including $N1+N2$ atoms and has two identical interfaces with area S; the energies $E_{\text{MgO}}^{\text{bulk}}$ and $E_{\text{TiN}}^{\text{bulk}}$ are the bulk total energy per atom for MgO and TiN, respectively. The two bulk energies are calculated using a supercell of the same size and in exactly the same manner, in particular, with the same set of k points.

The interface spacing range and energy obtained from the $(5+5)$ superlattices calculation are given in Table II. The energy differences among the three modes (modes I, II and IV; mode III will be discussed in Sec. III C) suggest that the Mg-N, Ti-O configuration (mode I) is energetically favorable. The optimized interface spacing between TiN and MgO interface layer is in range of 2.185 Å (Mg-N)–2.301 Å (Ti-O) because the interfacial interaction forces between cations and anions are different after relaxation. It is therefore believed that the cations ''prefer'' to bond with the anions across the interface due to an electrostatic reason.

Based on this growth mode, pseudopotential calculations on the interfaces were performed using the supercell of TiN(n)/MgO(n) ($n=3$, 5, and 7) in order to test the convergence of our results. The convergence of the interface energies with respect to the number of layers was checked through repeating PW91 calculations. The computing for the superlattice of TiN(n)/MgO(n) ($n=3$, 5, and 7) gives 0.283, 0.299, and 0.319 J/m^2, respectively, implying the calculations are converged to about 0.02 J/m^2. No significant difference in interface energy was observed between $5+5$ superlattice calculations and those made on supercells containing three or seven layers of TiN and MgO.

C. Discussion

For mode I, II, and IV, when relaxed, the number of geometry steps can be reduced quickly to reach a value of total energy for the equilibrium configurations, although the interfacial relaxation of mode I is slightly slowed. However, for mode III, at first, the number of energy gradient is not much reduced because the larger geometry steps require more cycles for the wave function to converge. The geometry trajectory shows that the supercell has a glide line in the [010] direction and forms a structure positioned almost in cation-anion bonding across the TiN/MgO(001) interface. Then, the number of geometry steps began to reduce quickly. In the later stages of the optimization, the step lengths are to meet the requirement of equilibrium structure. Finally, a new equilibrium interfacial structure is stably formed, which is cation-anion bonding.

Before relaxation, the interface energy of mode III is 2.411 J/m^2 by a single-point energy calculation, which can be obtained according to Eq. (1). In this case, the interface spacing is a setting value 3.280 Å (see Table II): After geometry optimization, mode III can be changed into the structure like mode I whose interface energy is 0.452 J/m^2 and interface spacing is in range of 2.187 Å (Mg-N)–2.297 Å (Ti-O) (almost equal to that of mode I) (see Table II). Although the value 0.452 J/m^2 is of same order of magnitude as the mode I interface energy, it is about 1.5 times more than that of mode I. This led us find that the relaxed mode III structure positions are not exactly in same (010) plane; there are po-

TABLE II. Interface spacing range and energy for different modes of the $5+5$ supperlattice.

Configuration	Equilibrium TiN-MgO spacing range (Å)	Interface energy (J/m^2)	Relaxation
Mode I	2.185~2.301	0.299	Yes
Mode II	3.711~3.934	2.232	Yes
Mode IV	3.258~3.467	2.065	Yes
Mode III	3.280 (setting value)	2.411	No
	2.187~2.297	0.452	Yes

sition undulations ($\leqslant 0.51\%$) along the [010] direction which worked a larger interface energy than mode I.

These results explain that mode II and IV interfacial structures are equilibrium but unfavorable. Mode I is not only at equilibrium but also stable; nevertheless, mode III is unstable, and disequilibrated, and would be changed toward mode I. Geometry optimization indicates that, in mode III, there is an interface stress determined by electrostatic interaction. Interface relaxation can strongly reduce the interface stress.

On the basis of mode I, we further calculated layer spacings within the $5+5$ supercell. Layers are numbered according to the order of its distance from the interface. For the TiN part, the mean spacing between the first and second layers is $2.062(d_1)$, and the spacing between the second and third layers is $2.114(d_2)$. As for the MgO part, the layer mean spacing between the first and second layers is 2.166, and between the second and third layers is 2.155. The data show the picture of the oscillating contraction and expansion of interface sublayers. If Δd represents the difference between d_2 and the half of calculated lattice constant d (Table I) for bulk TiN (MgO), $\Delta d/d$ is only 0.002 (0.011). X-ray diffraction and cross-sectional high-resolution electron microscopy confirmed a relative change in planar distance, $\Delta d/d$, of approximately 0.007 between TiN and MgO.[2] The calculated $\Delta d/d$ between the second and the third layer in the $5+5$ superlattice is apparently in agreement with the $\Delta d/d$ obtained by experiment. These indicate that the planar distance far from the interface would approach the measured value for noninterfaces as the number of layers increases. In addition, the charges in the central layer (layer 3) have nearly reached the noninterface equilibrium values (Ti: 0.79; N: -0.79; Mg: 1.26; O: -1.26) for the $5+5$ superlattice. This means $n=5$ is large enough for the central layer of the superlattice to exhibit noninterface properties (bulklike regions). Thus, the interface layer in the $5+5$ unit cell can represent the real interface layer.

D. Electronic structure

At interface, the downward (upward) shift of the density of states (DOS) is an effect of the attractive (repulsive) electrostatic potential between atoms. The lowest band energy corresponds to the preference of an interface configuration. The total DOS of the TiN/MgO($n=5$) supercells, with respect to the Fermi level, for the three different modes (mode I, II, and IV), is compared in Fig. 4(a). It is seen that mode I gives the most downward shift, which means such an interface configuration is the most preferred one across the TiN/MgO(001) interface. Such a configuration should increase the chemisorption potential energy of TiN on MgO(001), and therefore decrease the reactivity of the interface. For the mode I configuration we see a pseudogap of about -17.0 eV, which results from the PDOS (projected density of states) shifts in the interface layers. Figure 4(b) shows a PDOS shift of the first MgO layer in the three grow modes. In Fig. 4(c) it is seen that PDOS of the first TiN layer in mode I is slightly shifted towards lower energy compared with other modes. Therefore, the mode I configuration is believed to be

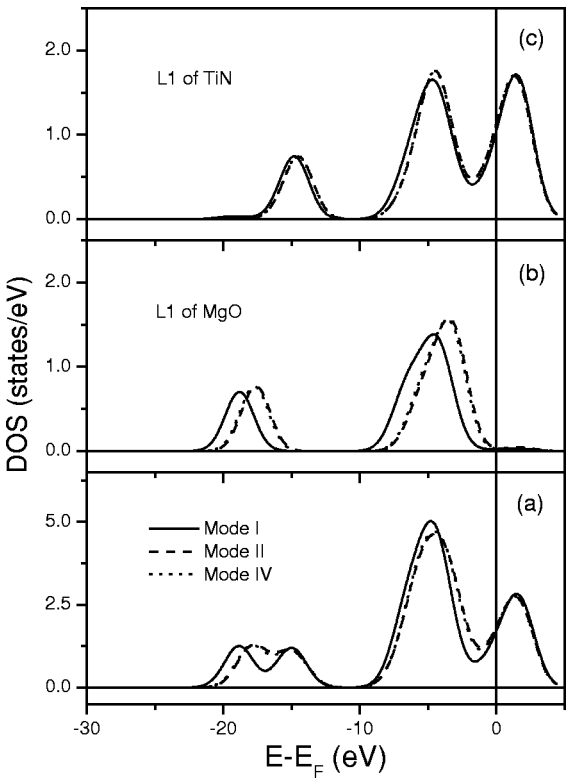

FIG. 4. Density of state calculated according to the three growth modes: (a) total density of states, (b) projected density of states (PDOS) of layer 1 of MgO, and (c) PDOS of layer 1 of TiN in the $5+5$ superlattice.

favorable not only because of the electrostatic contribution but also due to the band structure component.

On the basis of mode I, the projected partial DOSs was calculated for layers 1 and 3 of TiN in the $5+5$ superlattice, as shown in Fig. 5(a). The electron states, with their energy close to E_F, are mainly composed of N p-like electrons and Ti d-like electrons. It is seen that the electron states at the interface ($L1$) are almost same with that of noninterface area ($L3$). No states occur in the main band gap, however, there are low-energy states at the bottom of DOS in the TiN interface layer. They are the tails of Ti s- and p-like electron states at the energy range from -20 to -16 eV below E_F.

The projected partial DOSs of layers 1 and 3 of MgO in mode I of the $5+5$ superlattice is shown in Fig. 5(b). In the PDOS of MgO layer 1 (interface layer), the electron states with energy close to E_F are primarily from Mg s-like and O p-like electrons. The noninterface O atoms remain insulating, because of the lack of electron states at the Fermi level. The PDOS of O at interface is evidently different from that of O at the noninterface area, i.e., the structure of the $2p$ band of interface oxygen is somewhat perturbed. The interfacial hybridization with Ti results in some additional narrower width peaks and the extended tail from p electron states crossing E_F. The Mg PDOS is much smaller compared with that of the O atoms for the occupied states. Combining this with the fact that N p state lies well below $E_F(-10-0$ eV), the Mg-N interaction (mainly composed by p states between Mg and N atoms, there is nearly no s states interaction between Mg and N atoms) at interface should be much weaker than

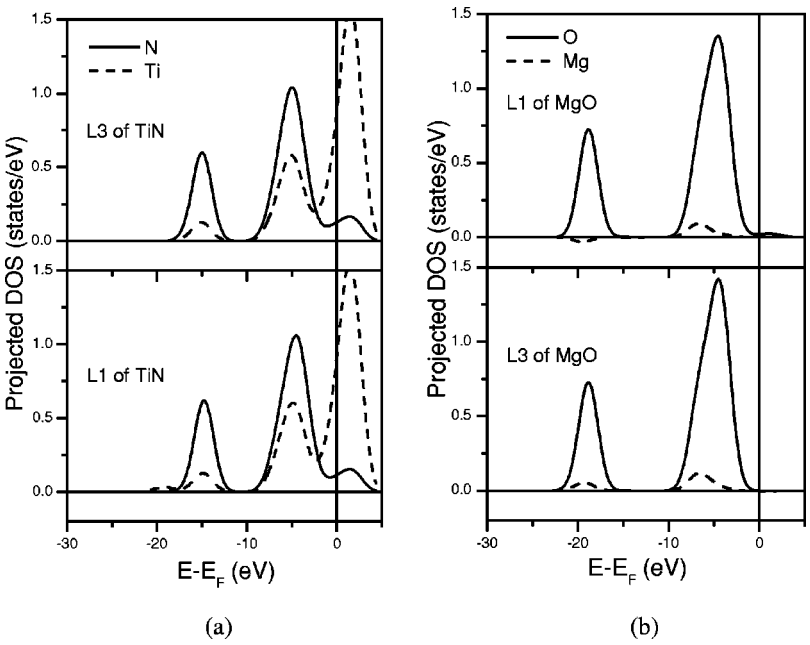

FIG. 5. (a) Projected density of states calculated for the layers 1 and 3 of TiN in the $5+5$ superlattice on the basis of mode I. (b) Projected density of states calculated for the layers 1 and 3 of MgO in the $5+5$ superlattice on the basis of mode I.

the Ti-O interaction. It reflects the covalent bond between Mg-N at interface is less than that between Ti-N. However, the calculated ionicity difference between Mg-N (2.46) at the interface is larger than that between Ti-O (1.66). As we know, the chemical interaction is composed of ionic and covalent bond. The result, optimized interface spacing between Mg-N (2.185 Å) less than that between Ti-O (2.301 Å) (see Table II), explains that the interfacial interaction force between Mg-N is larger than that between Ti-O, and reveals that the ionic contribution of the chemical interaction at interface plays a dominant role.

The electron densities with the energy range from 0.061 to 7.001 eV are plotted in Fig. 6. The contour plots in Figs. 6(a)–6(c) correspond to electron densities of mode I, II, and IV, respectively. It is again seen that the interfacial spacings are remarkably variant with growth modes. Figure 6(a) shows that mode I gives chemical bonding across the interface. On the contrary, no chemical bondings are formed at the interface with modes II and IV.

IV. CONCLUDING REMARKS

On the basis of high-resolution electron microscopy together with first-principle calculations, we have established interfacial fine structures at the interface of TiN/MgO (001). The following results are obtained.

(1) TiN thin film, grown on a MgO (001) substrate by molecular beam epitaxy, keeps parallel orientation relationships with MgO. The growth is epitaxial and the interface is coherent, as confirmed by electron diffraction and high-resolution images.

(2) Theoretical calculations based on the first-principle plane wave pseudopotential method have shown that cation-anion bonding (say, Ti-O and Mg-N) across the TiN/MgO(001) interface is favorable. The shortest interatomic spacing across the interface is found to be 2.185 Å for such configurations. The calculations have also shown that interfacial energy does not remarkably change with the thickness of TiN/MgO(001) supperlatice.

(3) Geometry optimization indicates that there is an interface stress determined by electrostatic interaction in mode III. Such an interface structure is unstable and disequilibrated, and would be changed toward mode I.

(4) The characteristic PDOS (projected densities of states) near the interface confirm that the cation-anion bonding configuration is preferred not only because of the electrostatic contribution but also due to the band structure component.

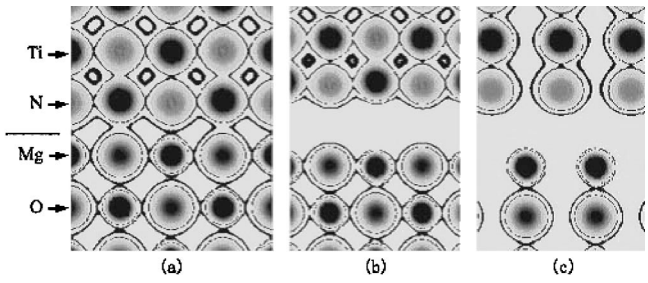

FIG. 6. The energy-sliced electron density distribution for (a) mode I at (010), (b) mode II at (010), and (c) mode IV at (110). Two contour lines were plotted at 0.25 eV (solid line) and 0.52 eV (dashed line).

ACKNOWLEDGMENTS

Thanks are given to the Hundred Talents Project of Chinese Academy of Sciences and National Outstanding Young Scientist Foundation for Grant No. 50325101 to X. L. Ma. The authors are grateful to Dr. J. Y. Wang, High-Performance Ceramic Division at this laboratory for computer resources and helpful discussions. We also gratefully acknowledge financial support from the Special Funds for the Major State Basic Research Projects of China (Grant No. 2002CB613503).

[1] Brian W. Karr, I. Petrov, David G. Cahill, and J. E. Greene, Appl. Phys. Lett. **70**, 1703 (1997).
[2] J. Bøttiger, J. Chevallier, J. H. Petersen, N. Schell, W. Matz, and A. Mücklich, J. Appl. Phys. **91**, 5429 (2002).
[3] X. L. Ma, N. Shibata, and Y. Ikuhara, J. Mater. Res. **14**, 1597 (1999).
[4] S. Miyagawa, K. Saitoh, H. Niwa, M. Ikeyama, G. Massouras, and Y. Miyagawa, J. Appl. Phys. **72**, 5663 (1992).
[5] K. Inumaru, T. Ohara, and S. Yamanaka, Appl. Surf. Sci. **158**, 375 (2000).
[6] Y. F. Zhukovskii, E. A. Kotomin, D. Fuks, S. Dorfman, and A. Gordon, Surf. Sci. **482-485**, 66 (2001).
[7] E. Heifets, Y. F. Zhukovshii, E. A. Kotomin, and M. Causá, Chem. Phys. Lett. **283**, 395 (1998).
[8] H. Furuya, I. Hirabayashi, Y. Yoshida, N. Matsunami, and Y. Takai, Physica C **378-381**, 965 (2002).
[9] J. Goniakowski, Phys. Rev. B **57**, 1935 (1998).
[10] M. C. Payne, M. P. Teter, T. A. Arias, and J. D. Joannopoulos, Rev. Mod. Phys. **64**, 1045 (1992).
[11] J. S. Lin, A. Qteish, M. C. Payne, and V. Heine, Phys. Rev. B **47**, 4174 (1993).
[12] H. J. Monkhorst and J. D. Pack, Phys. Rev. B **13**, 5188 (1976).
[13] M. P. Teter, M. C. Payne, and D. C. Allan, Phys. Rev. B **40**, 12255 (1989).
[14] D. Vanderbilt, Phys. Rev. B **41**, 7892 (1990).
[15] J. P. Perdew and Y. Wang, Phys. Rev. B **45**, 13244 (1992).
[16] M. Marlo and V. Milman, Phys. Rev. B **62**, 2899 (2000).
[17] P. Pulay, Mol. Phys. **17**, 197 (1969).
[18] O. L. Anderson, P. Andreatch, Jr., J. Am. Ceram. Soc. **49**, 404 (1966).
[19] M. I. McCarthy, N. M. Harrison, Phys. Rev. B **49**, 8574 (1994).
[20] A. De Vita, M. J. Gillan, J. S. Lin, M. C. Payne, I. Stich, and L. J. Clarke, Phys. Rev. B **46**, 12964 (1992).
[21] A. N. Baranov, V. S. Stepanyuk, W. Hergert, A. A. Katsnelson, A. Settels, R. Zeller, and P. H. Dederichs, Phys. Rev. B **66**, 155117 (2002).
[22] N. Schoenberg, Acta Chem. Scand. (1947–1973) **8**, 213 (1954).
[23] K. Kobayashi, Surf. Sci. **493**, 665 (2001).
[24] J. C. Grossmann, A. Mizel, M. Côté, M. L. Cohen, and S. G. Louie, Phys. Rev. B **60**, 6343 (1999).
[25] A. Šimůnek and J. Vackář, Phys. Rev. B **64**, 235115 (2001).
[26] R. Benedek, D. N. Seidman, and C. Woodward, J. Phys.: Condens. Matter **14**, 2877 (2002).